A&A 389, 556–567 (2002)
DOI: 10.1051/0004-6361:20011823

Astronomy & Astrophysics

Iron abundance in H II regions*

M. Rodríguez**

Instituto de Astrofísica de Canarias, 38200 La Laguna, Tenerife, Canarias, Spain***

Received 1 November 1999 / Accepted 20 December 2001

Abstract. Optical CCD spectra are used to determine the Fe abundances at several positions inside seven bright Galactic H II regions. The observed [Fe III] line ratios are compared with the predictions of different sets of collision strengths and transition probabilities for this ion to select the atomic data providing the best fit to the observations. The values found for the Fe^{++} and Fe^{+} abundances, along with ionization correction factors for the contribution of Fe^{3+}, obtained from available grids of photoionized models, imply that the Fe/O ratio in the ionized gas is between 2% and 30% of solar. The Fe abundances derived for each area are correlated both with the degree of ionization and the colour excess. A possible explanation is suggested, namely the presence of a population of small grains, probably originating from the fragmentation of larger grains. These small grains would release Fe atoms into the gas after the absorption of energetic photons; the small grains surviving this destruction process would be swept out of the ionized region by the action of radiation pressure or stellar winds. An indication of a further and more efficient destruction agent is given by the high Fe abundance derived for a position sampling the optical jet H 399 in M 20, where dust destruction due to shock waves has presumably taken place.

Key words. H II regions – ISM: abundances – dust, extinction

1. Introduction

The first reliable measurement of the Fe abundance in an H II region was carried out for M 42 by Osterbrock et al. (1992), who found Fe/H to be underabundant by a factor of 12 with respect to the solar value, confirming the previous estimate by Olthof & Pottasch (1975). Similar results were obtained for M 17 and M 8, for which Peimbert et al. (1993) found underabundance factors of 4 and 20, respectively. These values are consistent with the expected depletion of Fe on to the dust grains known to coexist with the ionized gas (Münch & Persson 1971; Osterbrock 1989), but the derived Fe abundances are significantly above the typical values for the undisturbed dense interstellar medium, ∼100 below solar (Jenkins 1987). This difference in the Fe depletion factors in H II regions and the interstellar medium is not readily explained, since refractory dust grains are expected to survive inside H II regions (Osterbrock 1989).

A possible explanation was offered in Rodríguez (1996), where the gaseous Fe abundances at different positions within seven Galactic H II regions were shown to be correlated with the degree of ionization, and this correlation was interpreted by relating the energetic photons with the release of Fe atoms from dust grains. This paper presents a more detailed and complete analysis of the data used in Rodríguez (1996) to determine the Fe abundances in M 42, M 43, M 8, M 16, M 17, M 20 and NGC 7635. The present analysis relies on recent atomic data for the determination of physical conditions and ionic abundances, and uses a somewhat different approach to derive the Fe abundance, leading to abundance values lower by about 40% than those presented in Rodríguez (1996). The correlation of the Fe abundance with the degree of ionization is confirmed to hold, as well as the further correlation with the colour excess, also previously presented in Rodríguez (1996). The implications that both results have for dust in H II regions are discussed.

2. The data

The results in this paper are based on the line intensities measured by Rodríguez (1996, 1999b) in the $\lambda\lambda$4200–8800 spectra of several positions within seven Galactic H II regions: M 42, M 43, M 8, M 16, M 17, M 20 and NGC 7635. This work centres on the Fe lines, but the values derived by Rodríguez (1999b) for some physical conditions and ionic abundances are also used: N_e[S II], the densities implied by the intensity ratio of [S II] lines $I(\lambda6716)/I(\lambda6731)$; T_e[N II], the temperatures derived from the intensity ratio of [N II] lines $I(\lambda6548+\lambda6583)/I(\lambda5754)$; and the ionic abundance

* Based on observations made with the Isaac Newton Telescope, operated on the island of La Palma by the Isaac Newton Group in the Spanish Observatorio del Roque de los Muchachos of the Instituto de Astrofísica de Canarias.

** e-mail: mrodri@inaoep.mx

*** *Present address*: Instituto Nacional de Astrofísica, Óptica y Electrónica INAOE, Apdo Postal 51 y 216, 72000 Puebla, Pue., México.

ratios N^+/H^+, O^+/H^+, O^{++}/H^+ and $O/H = O^+/H^+ + O^{++}/H^+$.

The ionization potentials for Fe^0, Fe^+, Fe^{++} and Fe^{3+} are 7.9, 16.2, 30.6 and 54.8 eV, respectively. Considering the excitation characteristics of the objects in the sample and the absence of He II λ4686 emission from all the nebular spectra (the ionization potential for He^+ is 54.4 eV) Fe^{3+} is not expected to be further ionized, and only Fe^+, Fe^{++} and Fe^{3+} should have appreciable concentrations within the ionized gas. Several [Fe III] and [Fe II] lines can be measured in the optical spectra of H II regions, but no optical [Fe IV] lines have been detected in H II regions and only one line has been measured in the UV spectra of an H II region: [Fe IV] λ2837 in M 42 (Rubin et al. 1997). Therefore, the values derived here for the Fe abundance are based on the Fe^+ and Fe^{++} abundances and ionization correction factors for the contribution of Fe^{3+} to the total abundance derived from available photoionization models.

3. [Fe III] lines

Up to twelve [Fe III] lines, previously listed and measured in M 42 by Osterbrock et al. (1992) and belonging to ($1F$), ($2F$) and ($3F$) multiplets, were detected in each object. At the achieved spectral resolution of 4 Å, [Fe III] λ4986 and [Fe III] λ4987 are blended; [Fe III] λ4607 is contaminated by O II λ4609 and N II λ4607 (Esteban et al. 1998); the intensity measured for [Fe III] λ4778 might have a small contribution from N II λ4780 (Esteban et al. 1999a), and [Fe III] λ4658 and [Fe III] λ5270 are appreciably blended in some objects with O II λ4661 and [Fe II] λ5273, respectively. On the basis of these considerations, [Fe III] λ4607 has been excluded from the abundance determination, [Fe III] λ4778 has been considered only in those positions where the abundance implied by this feature is consistent with the mean abundance implied by the other lines, and [Fe III] λ4658 and [Fe III] λ5270 have been used only for those objects where the contamination of these lines is negligible.

The reddening-corrected intensity ratios of the [Fe III] lines relative to Hβ are listed in Table 1 for all the positions studied (see Rodríguez 1999b for the values of the parameters used in the extinction correction). The extinction corrections applied to the relative [Fe III] line intensities are very small, a few per cent in most cases, with a maximum of 30% for [Fe III] λ5270 in M 17. The accuracy of the line intensities in Table 1 may vary from 10–20% for the positions in M 42 to more than 50% for some cases, in particular for those positions where only one [Fe III] line could be measured.

4. Atomic data for [Fe III]

Keenan et al. (1992) derived the relative populations of the lowest 17 levels of the $3d^6$ configuration in Fe^{++} using the collision strengths of Berrington et al. (1991) and the transition probabilities of Garstang (1957). Further calculations of the collision strengths for this ion are reported by Zhang (1996), whereas new values for the transition probabilities for the forbidden transitions have been derived by Nahar & Pradhan (1996) and Quinet (1996). The new effective collision strengths, when compared with the previous values of Berrington et al. (1991), are enhanced by a factor of up to 2, whereas the three available sets of transition probabilities differ from each other by ∼30% for most transitions, with differences up to an order of magnitude or more for some transitions.

In order to compare the results implied by the most recent atomic data with the previous calculations of Keenan et al. (1992), the level populations for Fe^{++} have been calculated with the collision strengths reported by Zhang (1996) and the two recent sets of transition probabilities (Nahar & Pradhan 1996; Quinet 1996). All collisional and downward radiative transitions for the 34 levels of the $3d^6$ configuration have been considered; test calculations restricted to the lowest 17 levels considered by Keenan et al. (1992) are found to agree to within 10% with the 34-level calculations.

In Fig. 1 some observed and predicted [Fe III] line ratios are presented as a function of N_e[S II] (Rodríguez 1999b). The values found for T_e[N II] cover the range T_e[N II] = 7800–10 800 K (Rodríguez 1999b), but the predicted line ratios for any temperature in this range are similar, and only the calculations for T_e = 10 000 K are shown in Fig. 1. The [Fe III] line ratios measured by Osterbrock et al. (1992) and Esteban et al. (1998, 1999a) in M 42 and M 8 are also presented in this figure; note that the measurements of Esteban et al. (1998, 1999a), performed at high-resolution, can be considered the most reliable.

Figures 1a–e show some of the line ratios for which the different atomic parameters lead to the greatest differences. In general, all the atomic data fit the measured line ratios reasonably well, but the results in Figs. 1a and 1e suggest that the calculations based on the collision strengths of Zhang (1996) and the transition probabilities of Quinet (1996) lead to a better fit.

The best way to judge the accuracy of the atomic data is to consider the dispersion in the abundances implied by the different lines. The most accurate [Fe III] intensities are probably those measured by Esteban et al. (1998) in M 42. The abundances and dispersions implied by the intensities measured in their position 1 for the ten lines in Table 1 and the three combinations of atomic data considered here are the following: $Fe^{++}/H^+ = (3.5\pm0.8)\times10^{-7}$ (Keenan et al. 1992), $(2.5 \pm 0.3) \times 10^{-7}$ (Zhang 1996; Nahar & Pradhan 1996) and $(2.5 \pm 0.2) \times 10^{-7}$ (Zhang 1996; Quinet 1996). When the [Fe III] intensities measured in other regions are considered, similar results are obtained: the oldest atomic data lead in most cases to higher dispersions and 10 to 50% higher mean abundance values. The most recent collision strengths lead to essentially equal mean abundance values independently of the transition probabilities used, and the dispersions are similar for the two recent sets of transition probabilities, although the transition probabilities of Quinet (1996) lead in general to somewhat lower dispersions. Therefore, the collision strengths of Zhang (1996)

Table 1. [Fe III] line intensities and Fe^{++} abundance.

Object	$I(\lambda)/I(H\beta) \times 100$[a]										$Fe^{++}/H^+ \pm \sigma$
	λ4658	λ4702	λ4734	λ4755	λ4769	λ4778	λ4881	λ4986+7	λ5270	λ5412	
M 42 A–1	0.77	0.255	0.096	0.142	0.086	0.081:	0.32	0.056	blend	0.029	$(3.3 \pm 0.4) \times 10^{-7}$
M 42 A–2	0.69	0.208	0.082	0.132	0.071	0.061	0.263	...	blend	0.026	$(2.2 \pm 0.4) \times 10^{-7}$
M 42 A–3	0.64	0.189	0.065	0.113	0.065	0.029	0.255	...	blend	0.015	$(2.5 \pm 0.4) \times 10^{-7}$
M 42 A–4	0.72	0.23	0.090	0.153	0.074	0.064:	0.289	...	blend	0.021	$(2.7 \pm 0.4) \times 10^{-7}$
M 42 A–5	0.72	0.20	0.074	0.132	0.047	0.042	0.25	...	blend	0.015:	$(3.6 \pm 0.6) \times 10^{-7}$
M 42 A–6	0.685	0.21	0.06	0.14	...	...	0.249	...	blend	...	$(2.5 \pm 0.2) \times 10^{-7}$
M 42 B–1	0.87	0.251	0.088	0.179	0.081	0.052	0.352	0.065	blend	0.031	$(4.2 \pm 0.7) \times 10^{-7}$
M 42 B–2	0.905	0.248	0.110	0.186	0.094	0.047	0.364	0.05:	blend	0.023	$(4.7 \pm 0.8) \times 10^{-7}$
M 42 B–3	0.85	0.219	0.067	0.18	0.074	0.052	0.309	0.053:	blend	0.018	$(4.2 \pm 1.0) \times 10^{-7}$
M 42 B–4	1.34	0.384	0.149	0.262	0.128	0.083	0.518	0.118	blend	0.053	$(6.7 \pm 1.0) \times 10^{-7}$
M 42 B–5	0.894	0.25	0.07	0.14	0.08	0.05	0.287	0.11	blend	...	$(4.8 \pm 1.1) \times 10^{-7}$
M 42 B–6	0.90	0.26	0.08	0.146	0.10	0.06	0.33	0.08	blend	0.038	$(4.9 \pm 0.7) \times 10^{-7}$
M 43–1	0.8	0.16	...	0.19	...	...	0.24	0.178:	blend	...	$(8.6 \pm 1.9) \times 10^{-7}$
M 43–2	0.81	0.23	...	0.33:	...	...	0.249	0.18:	blend	...	$(8.6 \pm 0.9) \times 10^{-7}$
M 43–3	0.6	...	...	0.12	...	...	...	0.21	blend	...	$(5.5 \pm 0.9) \times 10^{-7}$
M 43–4	0.83	0.21	...	0.19	...	...	0.209	0.164:	blend	...	$(9.4 \pm 1.2) \times 10^{-7}$
M 43–5	0.94	0.18	...	0.19	...	...	0.32	0.17:	blend	...	$(1.0 \pm 0.2) \times 10^{-6}$
M 8–1	0.57	0.18	0.07	0.11	0.06	...	0.25	0.07	blend	...	$(3.2 \pm 0.4) \times 10^{-7}$
M 8–2	0.57	0.18	0.05	0.065	...	...	0.21	0.06	blend	...	$(3.1 \pm 0.9) \times 10^{-7}$
M 8–3	0.64	0.19	...	0.13	0.04	...	0.23	...	blend	...	$(3.7 \pm 0.7) \times 10^{-7}$
M 8–4	0.55	0.19	0.05	0.10	0.037	0.02	0.178	0.052	blend	...	$(3.2 \pm 0.8) \times 10^{-7}$
M 8–5	0.51	0.23:	...	0.11	...	...	0.15	0.09	blend	...	$(3.5 \pm 1.1) \times 10^{-7}$
M 8–6	0.57	0.11	...	...	...	...	0.11	0.10	blend	...	$(2.3 \pm 0.5) \times 10^{-7}$
M 16–1	0.17	...	...	0.06	...	...	0.044	...	blend	...	$(1.5 \pm 0.8) \times 10^{-7}$
M 16–2	...	...	...	...	...	...	...	0.31	...	...	2.0×10^{-7}
M 17–1	blend	...	...	...	...	...	0.039	...	0.125	...	$(1.2 \pm 0.5) \times 10^{-7}$
M 17–2	blend	...	...	0.08	...	...	0.07	...	0.12	...	$(1.5 \pm 0.5) \times 10^{-7}$
M 17–3	blend	...	...	...	...	...	0.07	...	0.095	...	$(1.3 \pm 0.3) \times 10^{-7}$
M 20–1	1.0	0.18	...	0.19	...	...	0.30	0.29:	blend	...	$(7.8 \pm 1.9) \times 10^{-7}$
M 20–2	0.3	...	...	...	...	...	0.04	0.23	blend	...	$(2.2 \pm 0.6) \times 10^{-7}$
M 20–3	0.4	...	...	...	...	...	...	...	...	...	2.9×10^{-7}
NGC 7635–1	0.14	0.06	...	...	...	...	0.122	0.04	blend	...	$(1.7 \pm 0.6) \times 10^{-7}$
NGC 7635–2	0.39	0.11	...	0.08	...	...	0.18	0.046	blend	...	$(2.5 \pm 0.2) \times 10^{-7}$
NGC 7635–3	0.38	...	...	0.07	...	...	0.11	0.04	blend	...	$(2.1 \pm 0.3) \times 10^{-7}$

[a] [Fe III] λ4658 and [Fe III] λ5271 are blended with O II λ4661 and [Fe II] λ5273, respectively. The line intensities marked with colons imply abundance values that deviate by more than 50% from the mean value derived from the other lines and have been excluded from the abundance determination.

and the transition probabilities of Quinet (1996) will be used hereafter to derive the Fe^{++} abundances.

5. Fe^{++}/H^+

The last column in Table 1 shows the values of Fe^{++}/H^+ derived at each position from the measured [Fe III] intensities by using the collision strengths of Zhang (1996), the transition probabilities of Quinet (1996), the H I emissivities of Hummer & Storey (1987) and the physical conditions T_e[N II], N_e[S II] (Rodríguez 1999b). The dispersions in the abundances implied by the different lines considered are also indicated in Table 1; it can be seen that most of them are quite low, in the range 10–20%.

The values derived for Fe^{++}/H^+ are lower than those presented in Rodríguez (1996) by 10–70%. Up to 20% in these differences is due to the new values of the physical conditions implied by updated atomic data (Rodríguez 1999b); the remaining differences arise from the use of the most recent atomic data for Fe^{++}.

6. [Fe II] emission and Fe^+ abundance

Many lines of [Fe II] have been identified in the optical spectra of H II regions (see, for example, Osterbrock et al. 1992; Rodríguez 1996; Esteban et al. 1998, 1999a). Most of these lines are severely affected by fluorescence

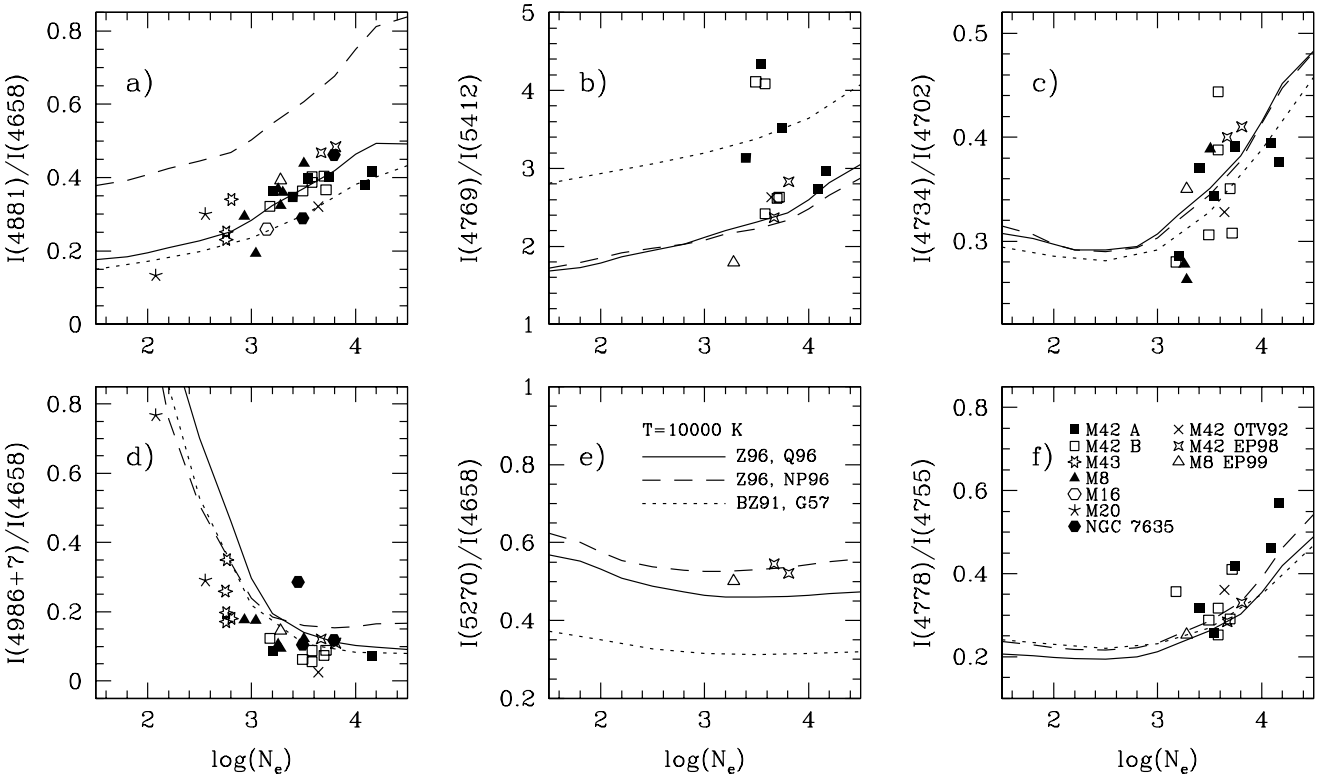

Fig. 1. Several observed [Fe III] line ratios are presented as a function of density, N_e[S II], and compared with the collisional excitation predictions for $T_e = 10\,000$ K. The atomic data used in the calculations are identified in panel **e)**, where Z96, Q96, NP96, BZ91 and G57 stand for Zhang (1996), Quinet (1996), Nahar & Pradhan (1996), Berrington et al. (1991) and Garstang (1957), respectively. The symbols representing the different H II regions are identified in panel **f)**, where OTV92, EP98 and EP99 identify the measurements performed by Osterbrock et al. (1992) and Esteban et al. (1998, 1999a).

effects (Rodríguez 1999a), but an estimate of the contribution of Fe^+ to the total Fe abundance can be obtained from the intensity measured for [Fe II] λ8617, which is almost insensitive to the effects of UV pumping (Lucy 1995; Baldwin et al. 1996). The reddening-corrected intensities of [Fe II] λ8617 relative to Pa12 or Pa13 are listed in Table 2; the applied extinction corrections are below 10%, and the uncertainties in the relative intensities may vary widely from ∼15% in M 42 to more than 50% in M 20–2, M 16 and M 17. The values of Fe^+/H^+ have been derived from the intensities in Table 2 by using the emissivities for [Fe II] (Bautista & Pradhan 1996) and H I (Hummer & Storey 1987) interpolated to the physical conditions T_e[N II] and N_e[S II].

In general, the values of Fe^+/H^+ are much lower than those found for Fe^{++}/H^+, as can be expected from the low ionization potential of Fe^+ (16.2 eV): most of the positions show $Fe^+/Fe^{++} \lesssim 0.3$ (see Table 2). One exception is M 43–3, where the Fe^{++}/H^+ abundance ratio is below those derived for the other positions in M 43, and the value of $Fe^{++}/H^+ + Fe^+/H^+$ turns out to be very similar. The most notable exceptions are M 20–1 and M 20–2, where $Fe^+/Fe^{++} \sim 1$. The spectra obtained for M 20 are very noisy in the wavelength range around [Fe II] λ8617 and the intensity measured for this line is uncertain by a factor of 2 in M 20–2, but in position M 20–1 all the [Fe II] and [Fe III] lines are relatively strong and the intensity of [Fe II] λ8617 has a much lower uncertainty. Position M 20–1 samples the optical jet HH 399, where the conditions could differ from those found in other regions (see the discussion in Sect. 7.1).

It has been suggested (Bautista & Pradhan 1998, and references therein) that most of the [Fe II] emission in M 42 and other H II regions originates in partially ionized layers with densities $N_e \sim 10^6$ cm^{-3}, much higher than those measured in the fully ionized zones, where $N_e \leq 10^4$ cm^{-3}, but several arguments have been presented against this hypothesis (Baldwin et al. 1996; Esteban et al. 1999b; Rodríguez 1999a; Verner et al. 2000). In any case, the [Fe II] lines measured in the near-infrared spectrum of M 42 have been found to arise in regions of moderate density (Marconi et al. 1998; Luhman et al. 1998), similar to the densities measured from the usual diagnostics based on [S II], [O II] or [Cl III] lines, and the [Fe II] λ8617 intensity measured in M 42, when compared with the intensities of these infrared lines, implies a common origin at moderate densities (see, for example, Fig. 5d in Bautista & Pradhan 1998). Hence, the calculation of the Fe^+/H^+ abundance ratio from [Fe II] λ8617 for the physical conditions T_e[N II] and N_e[S II] seems quite reasonable.

Another source of uncertainty in the values of Fe^+/H^+ in Table 2 arises from the atomic data used for Fe^+ – particularly the collision strengths. The Fe^+ abundances have

Table 2. [Fe II] λ8617 intensities and Fe^+ abundance.

Object	$I/I(H\,I)$	H I	Fe^+/H^+	Fe^+/Fe^{++}
M 42 A–1	0.094	Pa12	7.8×10^{-8}	0.24
M 42 A–2	0.09	Pa12	5.9×10^{-8}	0.27
M 42 A–3	0.030	Pa12	2.4×10^{-8}	0.10
M 42 A–4	0.061	Pa12	4.5×10^{-8}	0.17
M 42 A–5	0.048	Pa12	4.5×10^{-8}	0.13
M 42 A–6	0.038	Pa12	2.9×10^{-8}	0.12
M 42 B–1	0.088	Pa12	7.9×10^{-8}	0.19
M 42 B–2	0.044	Pa12	4.1×10^{-8}	0.09
M 42 B–3	0.055	Pa12	5.2×10^{-8}	0.12
M 42 B–4	0.159	Pa12	1.4×10^{-7}	0.21
M 42 B–5	0.08	Pa12	8.5×10^{-8}	0.18
M 42 B–6	0.101	Pa12	9.8×10^{-8}	0.20
M 43–1	0.095	Pa12	1.7×10^{-7}	0.20
M 43–2	0.157	Pa12	2.7×10^{-7}	0.31
M 43–3	0.21	Pa12	3.6×10^{-7}	0.65
M 43–4	0.085	Pa12	1.6×10^{-7}	0.17
M 43–5	0.08	Pa12	1.4×10^{-7}	0.14
M 8–1	0.021	Pa12	2.0×10^{-8}	0.06
M 8–2	0.027	Pa12	3.0×10^{-8}	0.10
M 8–3	0.024	Pa12	2.5×10^{-8}	0.07
M 8–4	0.013	Pa12	1.5×10^{-8}	0.05
M 8–5	0.019	Pa12	2.6×10^{-8}	0.07
M 8–6	0.02	Pa12	2.2×10^{-8}	0.10
M 16–1	0.015	Pa12	1.9×10^{-8}	0.13
M 16–2	...	...	...	...
M 17–1	0.009	Pa12	1.1×10^{-8}	0.09
M 17–2	...	...	...	...
M 17–3	0.016	Pa13	1.5×10^{-8}	0.12
M 20–1	0.5	Pa12	7.7×10^{-7}	0.99
M 20–2	0.1	Pa12	1.9×10^{-7}	0.86
M 20–3	...	...	...	...
NGC 7635–1	0.051	Pa12	5.9×10^{-8}	0.35
NGC 7635–2	0.066	Pa12	6.7×10^{-8}	0.27
NGC 7635–3	0.06	Pa13	5.1×10^{-8}	0.24

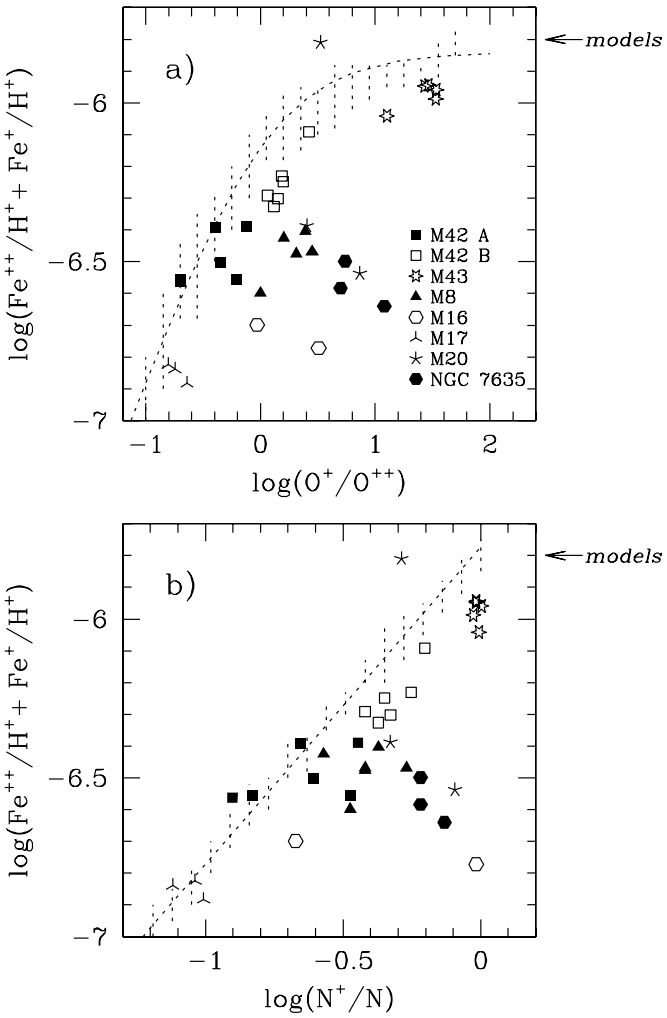

Fig. 2. The mean values of $Fe^+/H^+ + Fe^{++}/H^+$ are presented as functions of the degree of ionization given by **a)** O^+/O^{++} and **b)** N^+/N, with $\log(N/H) = -4.35$. The relations given by Eqs. (1) and (2) are also shown, scaled to $\log(Fe/H) = -5.8$; The vertical dotted lines show the range covered by the individual models (references in the text). It has been assumed that for those positions where [Fe II] λ8617 could not be measured (see Table 2), Fe^+/H^+ has a negligible contribution.

been calculated with the emissivities derived by Bautista & Pradhan (1996) using their own collision strengths, although Bautista & Pradhan (1998) consider more accurate the collision strengths of Pradhan & Zhang (1993) and Zhang & Pradhan (1995). However, this other set of collision strengths would lead to very similar values (∼30% lower) for the Fe^+ abundance derived from [Fe II] λ8617. The collision strengths presented by Pradhan & Zhang (1993) and Zhang & Pradhan (1995) can also be affected by uncertainties (Rodríguez 1999a; Oliva et al. 1999), but the contribution of Fe^+ to the total abundance is low and these uncertainties will not affect significantly the derived Fe abundances. The Fe abundance could be alternatively derived from the values of Fe^{++}/H^+ and ionization correction factors. This is the approach followed in Rodríguez (1996), and leads to very similar results.

7. Fe abundance

The values of $\log(Fe^{++}/H^+ + Fe^+/H^+)$ are presented as functions of the degree of ionization, $\log(O^+/O^{++})$ and $\log(N^+/N)$, in Fig. 2, where $\log(N/H) = -4.35$ has been assumed to hold for all the nebulae (Rodríguez 1999b). Figure 2 shows that $Fe^{++}/H^+ + Fe^+/H^+$ decreases with increasing degree of ionization for the positions in M 42 and M 17, reflecting the expected increment in the contribution of Fe^{3+} to the total abundance. However, the regions with lower degree of ionization – excluding M 43 – show unexpectedly low values of $Fe^{++}/H^+ + Fe^+/H^+$, that cannot be due to an error in the derived Fe^+/H^+ abundance ratio, as argued above and in Sect. 7.1.

Figures 2a and 2b also show an indication of the expected – i.e. model predicted – behaviour of the ionization fractions $x(Fe^{++}) + x(Fe^+)$ as a function of

$x(O^+)/x(O^{++})$ and $x(N^+)$, scaled to a total abundance $\log(Fe/H) = -5.8$. Two grids of ionization models have been used: those from Stasińska (1990) for solar metallicity $Z_\odot$ and for $Z_\odot/2$, and those from Gruenwald & Viegas (1992) for $Z_\odot$ and $Z_\odot/3$ (see Rodríguez 1999b for further details on the selected models). The vertical dotted lines in Figs. 2a and 2b show the range covered by the individual photoionization models; a further dotted line shows the assumed ionization correction factors, also scaled in these figures to $\log(Fe/H) = -5.8$, and given by:

$$Fe/H = 1.1 \times \left(O/O^+\right) \times \left(Fe^{++}/H^+ + Fe^+/H^+\right), \quad (1)$$

$$Fe/H = 0.94 \times \left(N/N^+\right) \times \left(Fe^{++}/H^+ + Fe^+/H^+\right). \quad (2)$$

These relations provide the correction for the contribution of Fe^{3+} to the Fe abundance in terms of the ionic and total abundances of O and N. According to the models, Eqs. (1) and (2) have accuracies better than ± 0.2 and ± 0.1 dex, respectively. Fe^{3+}, O^{++} and N^{++} are formed at 30.6, 35.1 and 29.6 eV, and none of these ions is expected to be further ionized. Hence, the ionization correction factor based on N should be more reliable, but whereas the total O abundance can be derived from the O^+ and O^{++} abundances using optical observations, the total N abundance has to be estimated from N^+. Therefore, the results for both Fe/N and Fe/O are presented here, and Fe/H is obtained from Fe/O × O/H.

The real accuracy of Eqs. (1) and (2) is difficult to estimate. Even if the ionization and recombination cross-sections used by the models are reliable, the predicted ionic concentrations may show systematic departures from those prevailing in the observed objects due to the necessarily unrealistic radiation fields and nebular structures assumed in the modeling. The dependence of the results on the radiation field and the nebular structure can be minimized by comparing, for observations and models, ions whose ionization potentials are similar, as the ions of O and N are compared with the Fe ions in Eqs. (1) and (2). The dispersion shown by the models around these relations in Eqs. (1) and (2), may then reflect real second-order variations in the spectral distribution of the radiation field, the gas density or its metallicity. The concentrations of those ions with low ionization potentials (such as O^0, Fe^+ or even Cl^+ and He^+) or relatively high ones (such as Ar^{3+}) are, however, severely affected by the unrealistic radiation fields or nebular structures assumed by models, but the relative ionization fractions of those ions whose concentrations depend on the flux density of photons with energies of 30–35 eV – as in Eqs. (1) and (2) – seem quite reliable (Rodríguez 1999b). Furthermore, the Fe abundances will be more reliable when obtained from $Fe^+/H^+ + Fe^{++}/H^+$ than from Fe^{++}/H^+. The relations implied by Eqs. (1) and (2) are also similar to the results obtained from individual ionization models. The photoionization models presented by Baldwin et al. (1991) and Rubin et al. (1991a, 1991b) for two regions in M 42 agree with Eqs. (1) and (2) to within 0.25 dex. Finally, the model derived by Bautista & Pradhan (1998) also for M 42, which includes the most recent values for the photoionization cross-sections and recombination-rate coefficients for the Fe ions, agrees more closely with Eq. (1). In any case, to confirm the trends in Eqs. (1) and (2), further calculations involving these new ionization and recombination cross-sections for different model assumptions would be of interest.

The values derived for Fe/N, Fe/O and Fe/H are listed in Table 3 and shown as a function of degree of ionization in Fig. 3. The results are compared with the solar abundances in the right hand axes of Fig. 3, where the solar values are $\log(Fe/N)_\odot = -0.47$, $\log(Fe/O)_\odot = -1.37$ and $\log(Fe/H)_\odot = -4.50$ (Grevesse et al. 1996). The depletion factors implied by the Fe/N and Fe/O abundance ratios are broadly consistent, especially if it is taken into account that whereas no significant amount of N is expected to be present in dust (Sofia et al. 1994), about 25% of the O abundance (∼0.1 dex) may be depleted in refractory dust grains (Cardelli et al. 1996). However, the depletion factors implied by Fe/H are much lower, probably reflecting the difficulties related to the choice of the correct reference abundances. Several recent studies of the abundances of different elements in the interstellar medium and in B stars suggest that the abundances of O, C, N and Kr relative to H are ∼2/3 the solar values (e.g. Snow & Witt 1996; Cardelli & Meyer 1997; Sofia et al. 1997), and similar underabundances for O, N and other elements are found in Rodríguez (1999b) for all the objects studied here. If this result holds also for the Fe/H abundance ratio, the most reliable depletion factors must be those implied by the Fe/N or Fe/O abundance ratios.

The Fe abundances presented here are in general about 0.2 dex lower than the values derived by other authors (e.g. Osterbrock et al. 1992 for M 42; Esteban et al. 1998, 1999a for M 42 and M 8; Rodríguez 1996), reflecting the different atomic data and the slightly different ionization correction factors used. As an example, if the line intensities measured by Osterbrock et al. (1992) in M 42 are analysed with the same atomic data used here and the same procedure followed, their derived $\log(Fe/H) = -5.57$ (for $O^+/O^{++} \sim 1$) would change to $\log(Fe/H) = -5.83$ if their ionization correction factor, $Fe^{3+}/Fe^{++} = 2$, is used, and to $\log(Fe/H) = -5.92$ if Eq. (1) is used instead.

The values of the Fe abundance listed in Table 3 are highly sensitive to the [Fe III] atomic data (in particular the collision strengths) and to the assumed ionization correction factors. Zhang (1996) estimates uncertainties of 10–20% for the collision strengths used here to derive the Fe^{++} abundances so that, even if the uncertainties are somewhat higher, the contribution of Fe^{3+} to the total abundance seems to be the main source of uncertainty.

New atomic data for the ionization and recombination rates of the Fe ions, or for the rates of their charge-exchange reactions, could change the predicted variation of $x(Fe^+) + x(Fe^{++})$ with $x(O^+)/x(O^{++})$ or $x(N^+)$, but the effects can only be significant for the higher ionization regions where the contribution of Fe^{3+} to the total abundance dominates. For those regions, namely

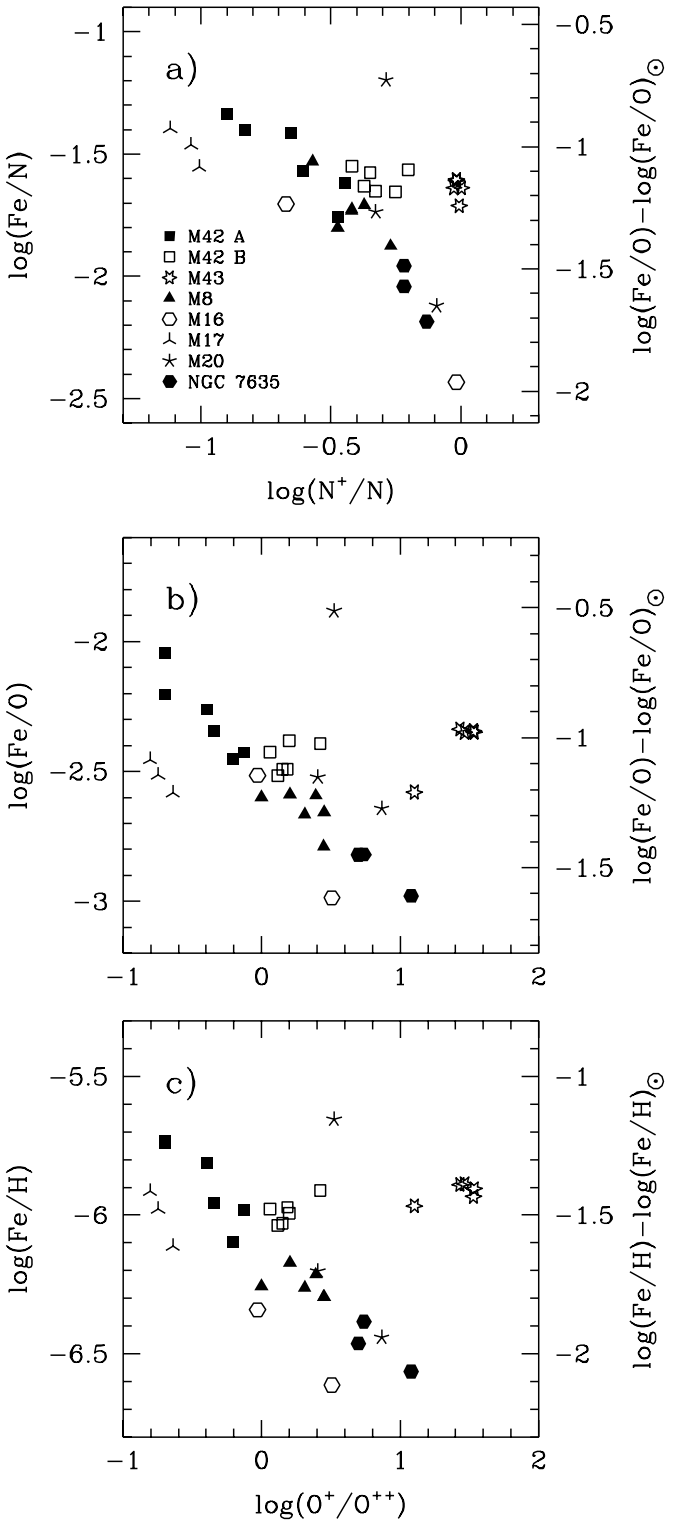

Fig. 3. The values of **a)** Fe/N, **b)** Fe/O and **c)** Fe/H, as derived from Eq. (1), Eq. (2) and the relation Fe/H = Fe/O × O/H. The values of Fe/H implied by the Fe/N abundance ratio can be obtained from: log(Fe/H) = log(Fe/N) − 4.35 (Rodríguez 1999b).

the positions in M 42 A and M 17, it might not be surprising to find Fe abundances similar to those in M 42 B, so that the trend in Fig. 3 would level off for $O^+/O^{++} < 1$.

Table 3. Fe abundances.

Object	Fe/N	Fe/O	Fe/H[a]
M 42 A–1	2.4×10^{-2}	3.7×10^{-3}	1.0×10^{-6}
M 42 A–2	1.7×10^{-2}	3.5×10^{-3}	8.0×10^{-7}
M 42 A–3	4.6×10^{-2}	6.3×10^{-3}	1.8×10^{-6}
M 42 A–4	2.7×10^{-2}	4.5×10^{-3}	1.1×10^{-6}
M 42 A–5	3.8×10^{-2}	5.5×10^{-3}	1.5×10^{-6}
M 42 A–6	4.0×10^{-2}	9.0×10^{-3}	1.8×10^{-6}
M 42 B–1	2.2×10^{-2}	3.2×10^{-3}	9.4×10^{-7}
M 42 B–2	2.8×10^{-2}	3.7×10^{-3}	1.0×10^{-6}
M 42 B–3	2.3×10^{-2}	3.1×10^{-3}	9.2×10^{-7}
M 42 B–4	2.7×10^{-2}	4.1×10^{-3}	1.2×10^{-6}
M 42 B–5	2.7×10^{-2}	4.1×10^{-3}	1.0×10^{-6}
M 42 B–6	2.4×10^{-2}	3.2×10^{-3}	1.1×10^{-6}
M 43–1	2.3×10^{-2}	4.5×10^{-3}	1.2×10^{-6}
M 43–2	2.6×10^{-2}	4.6×10^{-3}	1.3×10^{-6}
M 43–3	2.1×10^{-2}	2.6×10^{-3}	1.1×10^{-6}
M 43–4	2.3×10^{-2}	4.2×10^{-3}	1.2×10^{-6}
M 43–5	2.5×10^{-2}	4.5×10^{-3}	1.3×10^{-6}
M 8–1	1.9×10^{-2}	2.2×10^{-3}	5.1×10^{-7}
M 8–2	1.3×10^{-2}	1.6×10^{-3}	5.1×10^{-7}
M 8–3	2.0×10^{-2}	2.6×10^{-3}	6.1×10^{-7}
M 8–4	2.0×10^{-2}	2.2×10^{-3}	5.5×10^{-7}
M 8–5	2.9×10^{-2}	2.6×10^{-3}	6.7×10^{-7}
M 8–6	1.6×10^{-2}	2.5×10^{-3}	5.5×10^{-7}
M 16–1	3.7×10^{-3}	1.0×10^{-3}	2.4×10^{-7}
M 16–2	2.0×10^{-2}	3.1×10^{-3}	4.6×10^{-7}
M 17–1	2.8×10^{-2}	2.6×10^{-3}	7.7×10^{-7}
M 17–2	3.4×10^{-2}	3.5×10^{-3}	1.2×10^{-6}
M 17–3	4.0×10^{-2}	3.1×10^{-3}	1.0×10^{-6}
M 20–1	6.3×10^{-2}	1.3×10^{-2}	2.2×10^{-6}
M 20–2	1.8×10^{-2}	3.0×10^{-3}	6.3×10^{-7}
M 20–3	7.6×10^{-3}	2.3×10^{-3}	3.6×10^{-7}
NGC 7635–1	6.5×10^{-3}	1.0×10^{-3}	2.7×10^{-7}
NGC 7635–2	1.1×10^{-2}	1.5×10^{-3}	4.1×10^{-7}
NGC 7635–3	9.1×10^{-3}	1.5×10^{-3}	3.4×10^{-7}

[a] Derived from Fe/O × O/H.

However, the trend followed by the Fe abundances in the regions of lower ionization is established by the values derived for $Fe^{++}/H^+ + Fe^+/H^+$ (see Fig. 2) and seems quite robust. As discussed above, the real values of the depletion factors implied by the derived abundances, are somewhat uncertain, but nevertheless they imply that most of the Fe atoms remain in the dust. The different degrees of depletion factors found for the different objects seem to be well established, and the dependence of the results

on the ionization degree offers an explanation, since it relates those photons with energies $\gtrsim$35 eV to the release of Fe atoms from dust[1]. The implications of this result will be discussed in Sect. 8.

7.1. Comments on M 43 and M 20–1

The Fe abundance ratios derived for M 43 and M 20–1 show significant deviations from the relationship with the degree of ionization followed by the other objects. M 43 is the only region in the sample which is excited by a B-type star (NU Ori), its spectrum is greatly affected by dust-scattered stellar light, and is located several arc minutes to the north of M 42, belonging to the same molecular complex, although it is an independent H II region (Goudis 1982). The Fe/H abundance ratio in M 43 seems reliable since it is given by the calculated values for Fe^+/H^+ and Fe^{++}/H^+ and does not depend on ionization correction factors. A contribution of fluorescence effects, which are very important in M 43 (Rodríguez 1999a), to the [Fe II] λ8617 intensity cannot be an explanation, since when the Fe abundances are derived just from [Fe III] emission, which is not expected to suffer from fluorescence effects (Lucy 1995; Bautista & Pradhan 1998), the same deviation is found for M 43 (Rodríguez 1996). The relatively high Fe abundance in this object is not readily explained; maybe it is just an indication of the dependence of the Fe depletion on other factors apart from the radiation field: age, density, previous history, etc.

The deviation of M 20–1 from the relationships in Fig. 3 could be precisely reflecting the action of another factor. Position M 20–1 is located at the tip of HH 399, as mentioned above, a jet extending into the ionized gas from a molecular column in M 20 (Cernicharo et al. 1998; Hester et al. 1999). The jet is fully ionized and its spectrum is very similar to those measured for M 20–2 and M 20–3, yielding similar values for the physical conditions, chemical abundances and ionization fractions for all elements excluding Fe (Rodríguez 1999b). In fact, the only features showing distinct behaviour in the spectrum of M 20–1 are the [Fe III], [Fe II] and [Ni II] lines, whose intensities relative to Hβ are significantly higher than those measured for M 20–2 and M 20–3 (see Tables 1 and 2). Even the relative intensities of the [Fe II] lines, whose values reflect the effects of fluorescence in most [Fe II] lines (Rodríguez 1996, 1999a), depart in M 20–1 from the line ratios measured for the other objects. For example, the intensity ratio between [Fe II] λ4287, expected to be very sensitive to fluorescence, and [Fe II] λ8617, almost insensitive to pumping effects, is found to be lower in M 20–1 than in any other position, suggesting that fluorescence effects are minimal in this position. Therefore, although [Fe II] λ8617 could in principle be affected by fluorescence in some objects, the high values derived for Fe^+/H^+ and Fe^+/Fe^{++} in M 20–1 (the value of this latter ratio being above those found for lower-excitation objects like M 43 and NGC 7635), cannot be explained by resonance effects. The [Fe II] λ8617 line could only be measured in another position in this nebula (M 20–2), where Fe^+/Fe^{++} is found to be equally high, but since this line intensity is highly uncertain in M 20–2, it is not clear whether these values of Fe^+/Fe^{++} are characteristic of M 20 or are peculiar to the jet sampled in M 20–1 and imply a higher dust destruction efficiency in the lower ionization layers of the jet. In any case, a similar, although less extreme, Fe overabundance in M 20–1 can be found when the Fe abundances are calculated from just [Fe III] emission and model-predicted ionization fractions (Rodríguez 1996). This overabundance of Fe atoms in the gas, which has also been found for several typical, not fully ionized HH objects (Beck-Winchatz et al. 1996 and references therein), presumably reflects dust destruction due to shock waves arising from the interaction with the ionized gas of the material in the jet, which is estimated to move at a velocity of $\sim$370 km s^{-1} (Hester et al. 1999)[2].

7.2. [Fe IV] λ2837 and Fe^{3+} abundance

The only available measurement of an [Fe IV] line in an H II region is that performed by Rubin et al. (1997) for [Fe IV] λ2837 in M 42. Their measured reddening-corrected intensity ratio, $I(2837)/I(H\beta) \simeq 10^{-3}$, along with two previous photoionization models for two regions in M 42 and the collision strengths calculated by Berrington & Pelan (1995, 1996) for Fe^{3+}, imply $Fe/H = 4.6 \times 10^{-7}$ and 1.6×10^{-7} (with the difference between the two models' results being due mostly to their different predicted temperatures). These abundance ratios are significantly below $Fe/H = 3.0 \times 10^{-6}$, the value Rubin et al. (1997) consider consistent with [Fe II] and [Fe III] emission in M 42 and their models for this nebula.

The discrepancy is somewhat reduced if the abundances derived here from [Fe II] and [Fe III] lines (and more recent atomic data for [Fe III]) in M 42 are considered: $Fe/H = (0.8\text{–}1.8) \times 10^{-6}$. Although the weakness of the only measured [Fe IV] line, its sensitivity to temperature and the extinction correction may account for part of the discrepancy, it could be entirely due to errors in the collision strengths for Fe^{3+}. However, the more extensive calculations of the collision strengths for this ion performed by Zhang & Pradhan (1997) lead to very similar abundances. A 33-level model atom of Fe^{3+} based on the collision strengths of Zhang & Pradhan (1997) and the transition probabilities from Garstang (1958), for temperatures in the range 8000–8500 K and densities of several

[1] The degree of ionization is proportional to the number of energetic photons per electron (Osterbrock 1989), and since the distributions of gas and dust within a nebula are expected to follow a roughly similar pattern (see Münch & Persson 1971 for M 42), a higher gas density is likely to be associated with a higher dust concentration. Thus, the correlation can be interpreted as a relationship between the number of energetic photons available per dust grain and the amount of Fe released from dust.

[2] See also `http://eagle.la.asu.edu/hester/m20.html`

thousands (these physical conditions being in agreement with those usually measured in different zones in M 42 from [O III] and [Cl III] lines that should originate in the [Fe IV] emitting region: e.g. McCall 1979; Torres-Peimbert et al. 1980; Esteban et al. 1998; Rodríguez 1999b) and the intensity ratio measured for [Fe IV] λ2837 by Rubin et al. (1997), gives $Fe^{3+}/H^+ \simeq 2 \times 10^{-7}$. This value is a factor of 2–8 lower than the Fe^{3+} abundances implied by the results presented here for M 42 in Fig. 3c and Table 3: $Fe^{3+}/H^+ = (4\text{–}15) \times 10^{-7}$. The discrepancy is merely of a factor of $\sim$2 if only M 42 A–1 and M 42 A–2, located only 8.″5 south of the position observed by Rubin et al. (1997), are considered. Given all the uncertainties related to the determination of Fe^{3+}/H^+ from just one UV, weak [Fe IV] line measured in only one position whose optical spectra and [Fe II] and [Fe III] line intensities are not available at the moment, and given the wide range covered by the values derived here for Fe/H in M 42 and their uncertainties, a discrepancy of a factor $\geq$2 might not be significant.

Taken at face value, the discrepancy could indicate a failure in the model predictions for the Fe ionization fractions and a corresponding uncertainty in the Fe abundances derived for high-ionization H II regions. It has also been suggested that the lower Fe abundance implied by the [Fe IV] line could be real, reflecting the presence of a gradient in the gaseous abundance of this element (Bautista & Pradhan 1998), but the uncertainties related to the determination of the Fe^{3+} abundance are currently too high to reach any definite conclusion. Further studies of [Fe III] and [Fe II] lines at the position where [Fe IV] λ2837 has been observed and an assessment of the accuracy of the atomic data for Fe^{3+} will be needed to reach a full understanding of [Fe IV] emission in H II regions.

8. Fe abundance, extinction and dust in H II regions

8.1. Fe abundance and dust destruction

The high depletion factors measured for Fe in the interstellar medium and the high cosmic abundance of this element imply that Fe must contribute a substantial amount of mass to the dust grains (Sofia et al. 1994). Therefore, the degree of incorporation of Fe atoms to dust should give a good indication of the dust-to-gas ratio. Since the seven H II regions studied here have similar chemical abundances for those elements usually found in the gas phase (Rodríguez 1999b), it will be assumed that the Fe total abundance, i.e. in gas and dust, is the same for all these objects. The Fe abundance values derived here can then be compared to a reference Fe abundance to determine the fraction of Fe atoms present in the gas and depleted into dust for each area considered. Taking the solar Fe abundance as reference, the values derived for Fe/H or Fe/N imply that about 0.8–6% or 1–19% of the Fe atoms have been released to the gas phase. The corresponding logarithmic depletion factors, shown in Fig. 3, fall between the values typically found for cool clouds in the Galactic disc, where $\log(Fe/H) - \log(Fe/H)_\odot \simeq -2.09$ to -2.27, and those measured in the Galactic halo, which are in the range $\simeq -0.58$ to -0.69 (Savage & Sembach 1996). The relatively high Fe abundances in the halo are similar to the values found for high-velocity clouds, and this difference in the Fe depletion factors for cool disc and halo clouds (and the intermediate values found for warm disc clouds and clouds sampling both the disc and the halo) is interpreted as reflecting the action of the primary dust destruction agent: shock waves due to supernovae.

The Fe abundances derived here imply that most of Fe remains in the dust grains inside H II regions, but also imply the release to the gas of a significant amount of these atoms from the dust grains originally located inside molecular clouds, where up to 100% of Fe is expected to be in the solid phase. Energetic photons, instead of shock waves, (excluding M 20–1, see Sect. 7.1) seem to be responsible for this dust destruction effect, as suggested by the correlation of the Fe abundances with the degree of ionization in Fig. 3. Two processes might be responsible for this effect: vaporization and optical erosion or photodesorption, both leading to the release of atoms or molecules from the grains after the absorption of photons. Optical erosion results from the ionization or excitation of a bonding electron of a molecule after the absorption of a photon; this mechanism is expected to destroy only the ice mantles on the grains, and the refractory grains should not be affected (Osterbrock 1989). [However, note that photodesorption cross-sections for metal atoms on dust grains are not known, and this process could be of importance.] Assuming then that sublimation is the process that releases Fe atoms to the gas, the grains containing these atoms cannot be classical, i.e. characterized by a homogeneous composition and structure and with radii $a \sim 0.1$ μm, since these classical particles are in thermal equilibrium with the radiation field and have temperatures $T \sim 100$ K according to the calculations and the estimates obtained from the observed infrared emission, whereas refractory particles have much higher evaporation temperatures: $T \geq 1000$ K. However, if the grains are small enough, $a \leq 0.03$ μm, they can undergo significant temperature fluctuations after the absorption of one or a few energetic photons. Several studies on the temperature fluctuations undergone by dust grains in different environments conclude that only very small grains, with $a \sim 10$ Å, reach temperatures high enough to be destroyed. As an example, Guhathakurta & Draine (1989) estimate that graphite or silicate grains with $a \sim 5$ Å located at 0.3 pc from a B3V star could reach temperatures $T \sim 2000$ K, would lose atoms through sublimation and have lifetimes of about 3×10^5 years (whereas the ages of H II regions are of the order of one million years). These small dust grains contain about one thousandth of the total dust mass (Sellgren 1984) and their destruction cannot explain the relatively high Fe abundances measured for M 42. Nevertheless, a further population of small grains could be located in larger composite grains. Interstellar

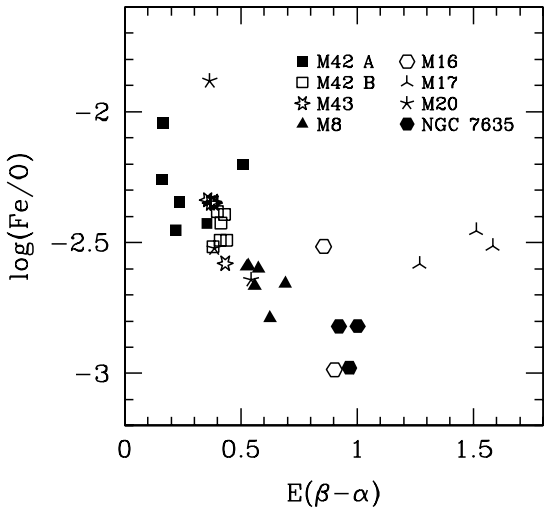

Fig. 4. The values of Fe/O as a function of the colour excess derived from the relative intensities of Hα and Hβ.

grains, and in particular those from molecular clouds, are expected to consist of loose aggregates of smaller subunits formed by an accretion process that might fragment once inside the ionized gas or at the ionization front.

As an example, PAH-like clusters within larger amorphous carbon grains could be easily released. Note that PAHs – polycyclic aromatic hydrocarbons, molecules of size ∼10 Å proposed to explain several emission bands observed in different environments such as the ionization fronts in H II regions – are destroyed inside H II regions (Bregman et al. 1989; Giard et al. 1994). PAHs or other kinds of aromatic molecules could aggregate and form conglomerates or amorphous carbon grains inside dense molecular clouds, and the abundant and chemically active Fe atoms might react with PAHs and accelerate the process. In fact, organometallic complexes could contain 5 to 10% of metal atoms in the interstellar medium and, thus, these complexes would play an important role in the depletion of heavy elements and in dust formation processes in the interstellar medium (Serra et al. 1992; Klotz et al. 1995).

8.2. Fe abundance and colour excess

The Fe/O abundance ratios are shown as a function of the colour excess implied by the relative intensities of the H I lines in Fig. 4, where it can be seen that there is a loose correlation between the two quantities. The correlation of Fe/H and Fe/N with $E(\beta-\alpha)$ is also apparent, although somewhat less markedly than that of Fe/O. Previously, Rodríguez (1996) presented the correlation of Fe/O with τ_β (the effective optical depth for extinction at Hβ), but the colour excess, which is an observed quantity, independent of the extinction law, is a more reliable and straightforward variable.

The positions in M 17 do not follow the correlation in Fig. 4, but this region is known to be heavily reddened by foreground dust, both interstellar and associated with the complex: Chini & Wargau (1998) estimate that $E(B-V) \sim 1$ mag is due to the diffuse interstellar medium in the line of sight to M 17 (note that $E(\beta-\alpha) \simeq E(B-V)$ when $R_V = A_V/E(B-V) \simeq 3$, the typical value for the diffuse interstellar medium) whereas the internal stars are further affected by $A_V > 3$ mag of local extinction. The positions studied in the other H II regions might be only slightly affected by external extinction due to a selection effect, since the observations were centred on the brightest positions of objects with high superficial brightness, but the difficulties inherent in disentangling the extinction components due to external and internal dust, preclude an estimate of the effects of interstellar extinction (i.e. unrelated to the complex) in the correlation presented in Fig. 4.

The extinction due to the interstellar medium along the line of sight to an H II region can be estimated by studying the stars projected on the nebula and assuming that those whose extinction law is similar to that usually found for the diffuse interstellar medium should be located in front of the stellar formation region. This is the method followed by Chini & Wargau (1998) for M 17, and it has also been applied to M 42, where Breger et al. (1981) find that $E(B-V) \simeq 0.05$ mag is due to interstellar extinction. The distinction between extinction due to internal dust and that due to external, associated dust is more difficult to make. However, taking into account the effects of scattering by dust internal to H II regions, this internal dust mixed with the ionized gas can produce a maximum colour excess $E(\beta-\alpha) \simeq 0.19$ mag (Gómez Garrido & Münch 1984). Therefore, the correlation in Fig. 4 relates the Fe abundance in the ionized gas – arising from dust destruction taking place in the region considered – with a colour excess necessarily due to foreground dust.

Given a volume of gas and dust, the spatial separation between the two components could be brought about through the effects of radiation pressure or stellar winds on the dust grains. However, collisional interactions and Coulomb forces between ions and charged particles tend to hold dust and gas together in H II regions. The efficiency of these processes depends on the size, structure and composition of the grains; the available calculations show that classical particles are strongly coupled to the gas (Osterbrock 1989). Small grains could be an exception: Cardelli & Clayton (1988) estimate that grains with sizes $a = 0.01$ μm initially located at a distance r from the central star can move under the effects of radiation pressure by $\Delta r/r \geq 0.2$ in 10^4 years. Since many H II regions are known to have complex structures, with dense clumps or molecular columns inside or in front of the ionized gas (e.g. M 8 and NGC 7635, as shown by their detailed HST images), the overall effect of radiation pressure or stellar winds could well be to push a significant amount of dust outside the nebula into our line of sight.

In conclusion, both correlations shown by the gaseous Fe abundance in H II regions seem to require the presence of dust grains differing from the classical grains due to their smaller sizes or loose structure. These non-classical

grains could contain 10–20% of the total Fe abundance, their destruction would be due to photons with energies above 35 eV and could take place after the fragmentation of an original composite grain. On the other hand, on a longer timescale, the surviving non-classical grains would be pushed outside the ionized region through the action of radiation pressure or stellar winds, where they would be responsible for most of the colour excess found in the objects studied here.

9. Conclusions

The spectra of several positions inside seven Galactic H II regions have been analysed to derive their Fe abundance. The relative intensities measured for the [Fe III] lines have been compared with the values predicted by three combinations of the available atomic data, and it has been shown that the collision strengths of Zhang (1996) and the transition probabilities of Quinet (1996) lead to the best agreement between the observed and predicted line ratios. The Fe^{++}/H^+ abundance ratios derived for all the positions studied with the above mentioned atomic data are 10–50% lower than the values implied by the calculations of Keenan et al. (1992), which are based on older atomic data and have been used in several previous studies of the Fe abundance in nebulae.

The Fe^+/H^+ abundance ratios have been calculated using the [Fe II] λ8617 line, which is almost insensitive to fluorescence, and the emissivities of Bautista & Pradhan (1996). The derived Fe^+ abundances may be affected by uncertainties in the measured intensities and in the collision strengths, but the effects of these uncertainties in the Fe abundances should be small, since the contribution of Fe^+ to the total abundance is very low for most positions. The Fe abundances are consequently derived from the values of $Fe^{++}/H^+ + Fe^+/H^+$ and ionization correction factors for the contribution of Fe^{3+} obtained from available grids of photoionization models.

The derived Fe/O abundance ratios are 3 to 40 times lower than the solar value, implying that most of the Fe atoms remain in dust grains inside the ionized volume. These underabundance factors are, however, significantly lower than those found for the undisturbed interstellar medium, where more than 99% of Fe is depleted into dust (Savage & Sembach 1996). The correlation between the calculated Fe abundances and the degree of ionization explains this difference by relating the energetic photons in H II regions with the release of Fe atoms from dust. Further agents can be responsible for dust destruction in H II regions, and a remarkable example is provided by position M 20–1, on the tip of the optical jet HH 399, where the Fe gaseous abundance is significantly higher than in the other areas, presumably indicating dust destruction due to the shock waves related to the jet.

The inferred dust destruction by photons, together with the correlation of the Fe abundance with the colour excess, can be explained by invoking the presence of loosely-bound dust grains or mantles, containing 10 to 20% of the Fe abundance, whose fragmentation would produce grains small enough to be destroyed by sublimation processes, whereas the remnants of these small grains would be swept out of the ionized region by radiation pressure or stellar winds.

The present results rely on the estimated contribution of Fe^{3+} to the total Fe abundance. The uncertainties related to this estimate, strengthened by the current difficulties in explaining [Fe IV] emission in M42, may cast some doubts on the validity of the results for the high ionization objects. Certainly, this issue should be resolved before the correlation between the Fe abundances and the degree of ionization can be considered as firmly established, thus favouring the proposed interpretation. If such were not the case, and the predicted contribution of Fe^{3+} to the total abundance were found to be grossly in error, the new results would surely lead to alternative scenarios for the evolution of dust in H II regions.

Acknowledgements. G. Münch suggested this project; I am greatly indebted to him and to A. Mampaso for their advice during its development. I also thank F. P. Keenan and S. N. Nahar for sending their data in electronic form, and M. A. Bautista for kindly providing the [Fe II] emissivities. I am grateful to T. Mahoney for revising the English text and to J. E. Beckman and W. Wall for some later corrections. I thank two anonymous referees for useful comments that have helped to improve this paper. This research has made use of NASA's Astrophysics Data System Abstract Service. A grant of the Spanish DGES PB97–1435–C02–01 provided partial support for this work.

References

Baldwin, J. A., Ferland, G. J., Martin, P. G., et al. 1991, ApJ, 374, 580
Baldwin, J. A., Crotts, A., Dufour, R. J., et al. 1996, ApJ, 468, L115
Bautista, M. A., & Pradhan, A. K. 1996, A&AS, 115, 551
Bautista, M. A., & Pradhan, A. K. 1998, ApJ, 492, 650
Beck-Winchatz, B., Böhm, K. H., & Noriega-Crespo, A. 1996, AJ, 111, 346
Berrington, K. A., & Pelan, J. C. 1995, A&AS, 114, 367
Berrington, K. A., & Pelan, J. C. 1996, A&AS, 119, 189 (Erratum)
Berrington, K. A., Zeippen, C. J., Le Dourneuf, M., Eissner, W., & Burk, P. G. 1991, J. Phys. B, 24, 3467
Breger, M., Gehrz, R. D., & Hackwell, J. A. 1981, ApJ, 248, 963
Bregman, J. D., Allamandola, L. J., Tielens, A. G. G. M., Geballe, T. R., & Witteborn, F. C. 1989, ApJ, 344, 791
Cardelli, J. A., & Clayton, G. C. 1988, AJ, 95, 516
Cardelli, J. A., & Meyer, D. M. 1997, ApJ, 477, L57
Cardelli, J. A., Meyer, D. M., Jura, M., & Savage, B. D. 1996, ApJ, 467, 334
Cernicharo, J., Lefloch, B., Cox, P., et al. 1998, Science, 282, 462
Chini, R., & Wargau, W. F. 1998, A&A, 329, 161
Esteban, C., Peimbert, M., Torres-Peimbert, S., & Escalante, V. 1998, MNRAS, 295, 401

Esteban, C., Peimbert, M., Torres-Peimbert, S., García-Rojas, J., & Rodríguez, M. 1999a, ApJS, 120, 113
Esteban, C., Peimbert, M., & Torres-Peimbert, S. 1999b, A&A, 342, L37
Garstang, R. H. 1957, MNRAS, 117, 393
Garstang, R. H. 1958, MNRAS, 118, 572
Giard, M., Bernard, J. P., Lacombe, F., Normand, P., & Rouan, D. 1994, A&A, 291, 239
Gómez Garrido, P., & Münch, G. 1984, A&A, 139, 30
Goudis, C. 1982, The Orion Complex: A case study of interstellar matter (Dordrecht: Reidel)
Grevesse, N., Noels, A., & Sauval, A. J. 1996, in ASP Conf. Ser. 99, Cosmic Abundances, ed. S. S. Holt, & G. Sonneborn (San Francisco: ASP), 117
Gruenwald, R. B., & Viegas, S. M. 1992, ApJS, 78, 153
Guhathakurta, P., & Draine, B. T. 1989, ApJ, 345, 230
Hester, J. J., Scowen, P. A., Stapelfeldt, K. R., & Krist, J. 1999, BAAS, 194.6810
Hummer, D. G., & Storey, P. J. 1987, MNRAS, 224, 801
Jenkins, E. B. 1987, in Interstellar Processes, ed. D. J. Hollenbach, & H. A. Thronson (Dordrecht: Reidel), 533
Keenan, F. P., Berrington, K. A., Burke, P. G., Zeippen, C. J., Le Dourneuf, M., & Clegg, R. E. S. 1992, ApJ, 384, 385
Klotz, A., Marty, P., & Boissel, P., et al. 1995, A&A, 304, 520
Lucy, L. B. 1995, A&A, 295, 555
Luhman, K. L., Engelbracht, C. W., & Luhman, M. L. 1998, ApJ, 499, 799
Marconi, A., Testi, L., Natta, A., & Walmsley, C. M. 1998, A&A, 330, 696
McCall, M. 1979, ApJ, 229, 962
Münch, G., & Persson, S. E. 1971, ApJ, 165, 241
Nahar, S. N., & Pradhan, A. K. 1996, A&AS, 119, 509
Olthof, H., & Pottasch, S. R. 1975, A&A, 43, 291
Oliva, E., Moorwood, A. F. M., Drapatz, S., Lutz, D., & Sturm, E. 1999, A&A, 343, 943
Osterbrock, D. E. 1989, Astrophysics of Gaseous Nebulae and Active Galactic Nuclei (Mill Valley: Univ. Science Books)
Osterbrock, D. E., Tran, H. D., & Veilleux, S. 1992, ApJ, 389, 305
Peimbert, M., Torres-Peimbert, S., & Dufour, R. J. 1993, ApJ, 418, 760
Pradhan, A. K., & Zhang, H. L. 1993, ApJ, 409, L77
Quinet, P. 1996, A&AS, 116, 573
Rodríguez, M. 1996, A&A, 313, L5
Rodríguez, M. 1999a, A&A, 348, 222
Rodríguez, M. 1999b, A&A, 351, 1075
Rubin, R. H., Simpson, J. P., Haas, M. R., & Erickson, E. F. 1991a, ApJ, 374, 564
Rubin, R. H., Simpson, J. P., Haas, M. R., & Erickson, E. F. 1991b, PASP, 103, 834
Rubin, R. H., Dufour, R. J., Ferland, G. J., et al. 1997, ApJ, 474, L131
Savage, B. D., & Sembach, K. R. 1996, ARA&A, 34, 279
Sellgren, K. 1984, ApJ, 277, 623
Serra, G., Chaudret, B., Saillard, Y., et al. 1992, A&A, 260, 489
Snow, T. P., & Witt, A. N. 1996, ApJ, 468, L65
Sofia, U. J., Cardelli, J. A., & Savage, B. D. 1994, ApJ, 430, 650
Sofia, U. J., Cardelli, J. A., Guerin, K. P., & Meyer, D. M. 1997, ApJ, 482, L105
Stasińska, G. 1990, A&AS, 83, 501
Torres-Peimbert, S., Peimbert, M., & Daltabuit, E. 1980, ApJ, 238, 133
Verner, E. M., Verner, D. A., Baldwin, J. A., Ferland, G. J., & Martin, P. G. 2000, ApJ, 543, 831
Zhang, H. L. 1996, A&AS, 119, 523
Zhang, H. L., & Pradhan, A. K. 1995, A&A, 293, 953
Zhang, H. L., & Pradhan, A. K. 1997, A&AS, 126, 373